

From Redundancy to Relevance: Enhancing Explainability in Multimodal Large Language Models

Xiaofeng Zhang¹, Chen Shen², Xiaosong Yuan², Shaotian Yan²,
Liang Xie², Wenxiao Wang², Chaochen Gu^{1*}, Hao Tang³, Jieping Ye²

¹Shanghai Jiao Tong University

²Alibaba Group

³Carnegie Mellon University
framebreak@sjtu.edu.cn

Abstract

Recently, multimodal large language models have exploded with an endless variety, most of the popular Large Vision Language Models (LVLMs) depend on sequential visual representation, where images are converted into hundreds or thousands of tokens before being input into the Large Language Model (LLM) along with language prompts. The black-box design hinders the interpretability of visual-language models, especially regarding more complex reasoning tasks. To explore the interaction process between image and text in complex reasoning tasks, we introduce the information flow method to visualize the interaction mechanism. By analyzing the dynamic flow of the information flow, we find that the information flow appears to converge in the shallow layer. Further investigation revealed a redundancy of the image token in the shallow layer. Consequently, a truncation strategy was introduced to aggregate image tokens within these shallow layers. This approach has been validated through experiments across multiple models, yielding consistent improvements.

1 Introduction

In the real world, reasoning also involves information in modalities other than text, with visual modalities being the most prevalent. Currently, a majority of popular multimodal large language models (MLLMs) rely on sequential visual representation, where images are transformed to hundreds or thousands of tokens when feeding to LLM together with language prompts [2, 6, 13, 19, 27], they are primarily trained to respond to instructions based on visual inputs, employing a decoder-only autoregressive design as a black box. Although these MLLMs exhibit impressive generation capabilities, the black-box design hinders the interpretability of visual-language models. It is very meaningful to explore the interpretability mechanisms of complex reasoning.

Some works have already commenced preliminary exploration into the caption mechanisms of LLMs [7–9, 12]. OPERA [41] addressed the potential causes of hallucinations in MLLMs by analyzing attention maps. During the inference phase, the model may produce hallucinations by sequentially summarizing previous tokens when processing certain key tokens such as ‘-’, ‘?’, and other symbols. OPERA mitigates these hallucinations by imposing penalty constraints on attention scores, marking the first work to visualize multimodal hallucinations. In addition, Fastv [42] identifies inefficiencies in attention mechanisms within MLLMs. The authors observed that the computation of attention for visual tokens in the deep networks of these models is extremely inefficient. While the previous studies have made significant strides in enhancing MLLMs perception and inference speed through leveraging attention-based mechanisms, they tend to focus less on the dynamic interplay of image-text

interactions. Recognizing this gap, our research aims to deepen the understanding of how images and texts influence each other within complex reasoning.

Understanding the flow of information between image and text tokens is crucial for dissecting multimodal complex reasoning. We define 'information flow' as the rate at which image, user, and system tokens influence the answer token. To observe dynamic changes in the information flow, we employ both Attention Score and Grad-CAM to represent dynamic changes effectively. Attention score highlights relevant regions through forward propagation, while Grad-CAM captures gradient changes through backward propagation, thus revealing the saliency of image features. These two methods complement each other and provide a comprehensive way to understand the dynamics of information flow. Specifically, Grad-CAM visualizes how the model processes image information at each layer, showing the image regions of interest in the model's decision-making process. Information flow is combined with attention scores in forward passes, where the attention scores reveal how the model selects and weights input elements (e.g., images and text) and the correlations between these elements at each layer.

This combination of Grad-CAM and attention score allows us to quantify how important different elements are and to see exactly where and what these elements do in the input data. This multi-perspective approach of looking at the model from multiple angles helps expose how the model works on the inside, making it easier to understand and revealing areas where it might be improved. As shown in Fig. 1, our observation indicates a convergence of information flow in the shallow layers (1-11), while this convergence is much less in the deeper layers (12-32).

Based on our observation of information flow convergence in the shallower layers, we further explore the saliency of image tokens in the shallower layers. Our analysis reveals that the model focuses on both relevant and irrelevant image features which leads us to speculate that the irrelevant image features could detract from the model's performance. To verify this hypothesis, we designed a truncation experiment. The experiment revealed that by truncating image tokens based on the attention weights, the model's inference accuracy increased. This demonstrates the existence of redundant features in image tokens within shallow layers. Moreover, our approach not only enhances the model performance by cutting down redundant features but also provides a novel perspective on the interpretability of multimodal large language models. In summary, the main contributions of our paper are as follows:

- In this paper, we combined Grad-CAM and attention-score to explore the interaction mechanisms and information flow in multimodal complex reasoning tasks. Experiments find that the image tokens at shallow layers have convergence on salient regions.
- Our analysis identified redundancy in the information flow of the image token in the shallow layer, for this reason, we proposed a truncation strategy to prune the image token according to the information flow to enhance the influence of the salient regions.

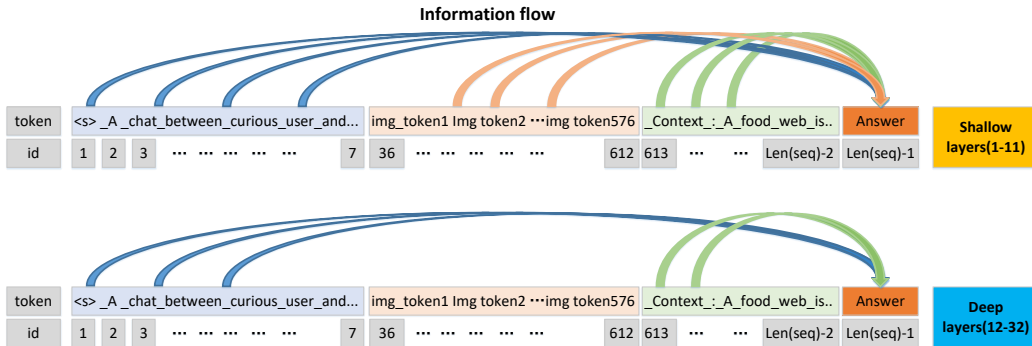


Figure 1: It shows the flow of attention-score, the information flow of tokens, from left to right are system tokens, image tokens, user tokens, and output tokens. There is a convergence of the information flow of the system token, image token, and user token towards the output token at the shallow layers. The convergence of the information flow of the system token and user token is much more obvious than the image token at the deep layers.

2 Related work

2.1 Multimodal large language models

Multimodal large language models are born out of the development of large models, whereas traditional multimodal models face huge computational overheads, LLMs have ‘prior knowledge’ about the world after extensive training, so a natural idea is to use LLMs as the prior knowledge and cognitive enabler for multimodal Large Models, which are usually performed on a large scale (relative to a pair of data). The representatives of LLMs are Flamingo, LLaVA(1.0, 1.5, 1.6), Qwen-VL, Internvl, miniGemini [1–3, 5, 6, 13–15, 17–27, 27, 29, 30]. These MLLMs are equipped with image understanding, long textual reasoning, and a complex inference system, and they have been widely used in the field of LLMs for many years.

2.2 Chain-of-Thought reasoning

LLM reasoning can be classified as mathematical reasoning, commonsense reasoning, symbolic reasoning, logical reasoning, and multimodal reasoning, according to [31]. In the real world, reasoning also involves information in modalities other than text, with visual modalities being the most prevalent. To this end, many benchmarks for visual multi-modal reasoning are proposed ([32–35]), and among them, ScienceQA ([35]) annotates the reasoning process and is the most commonly used visual multi-modal reasoning benchmark. MMCOT [36] combines linguistic (textual) and visual (image) modalities into a two-stage framework, separating rationale generation from the answer, and presenting implicit reasoning explicitly. DDCoT [37] maintains a critical attitude through negative spatial cues and incorporates multimodality into reasoning by dividing the reasoning responsibilities into inference and recognition and then incorporating the visual recognition capabilities of the visual model into joint reasoning. Visual-CoT [39] proposes a multi-turn processing pipeline that dynamically focuses on visual inputs and provides interpretable thoughts.

2.3 Explainable for multimodal large language models

Currently, most research focuses on instruction tuning large models, to develop models with higher input resolution, more complex functionalities (such as graph-based and text-based capabilities), stronger perceptual abilities, and finer granularity. However, there is a lack of studies that explain the internal mechanisms of multimodal large language models (MLLMs), which remain a black box. Recently, OPERA [41] addressed the potential causes of hallucinations in MLLMs by analyzing attention maps. During the inference phase, the model may produce hallucinations by sequentially summarizing previous tokens when processing certain key tokens such as ‘-’, ‘?’, and other symbols. OPERA mitigates these hallucinations by imposing penalty constraints on attention scores, marking the first work to visualize multimodal hallucinations.

Similarly, Fastv [42] identifies inefficiencies in attention mechanisms within large-scale visual language models (LVLMs), particularly in models such as LLaVA-1.5, QwenVL-chat, and Video-LLaVA. The authors observed that the computation of attention for visual tokens in the deep networks of these models is extremely inefficient. To address this, they proposed an image-token pruning strategy at specific layers, aiming for a sparser approach than that used for textual data processing.

While the previous studies have made significant strides in enhancing MLLMs perception and inference speed through leveraging attention-based mechanisms, they tend to focus less on the dynamic interplay of image-text interactions. Recognizing this gap, our research aims to deepen the understanding of how images and texts influence each other within complex reasoning.

3 The Proposed Method

To visualize the information flow, attention scores and Grad-CAM [10] are used to provide a comprehensive view of the information flow. Attention scores show the model’s forward processing path, while Grad-CAM offers insights into the backward path, reflecting the contribution of different input elements to the output. This combination method not only helps quantify the importance of input elements but also visualizes where and how these elements affect the model’s predictions.

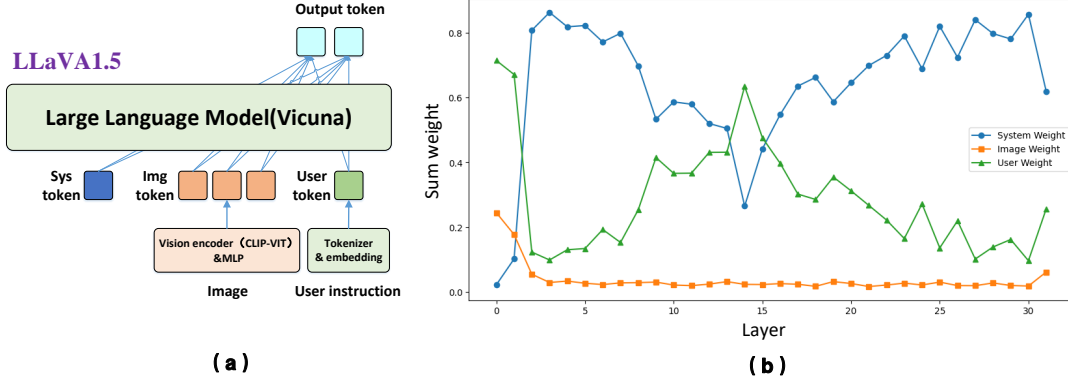


Figure 2: (a) is the structure of LLaVA1.5, (b) is the sum weight of several tokens in LLaVA1.5 (system tokens, image tokens, user tokens).

3.1 Grad-CAM for multimodal large language models

Our method is inspired by Grad-CAM [10], complex reasoning is still essentially a text generation task, and the answer generation is a sentence made up of the classification results for each word, i.e., the *cls* logits of all the individual words are added together, the network outputs probabilities for n tokens, denoted as $z = [z_i, ..z_n]$, to visualize the model’s output answer using Grad-CAM:

$$z_{\text{answer}} = \sum_i^n z_i, \quad (1)$$

to obtain the logits representing the overall output of the model. Then we derive the partial derivatives:

$$G_k = \frac{\partial z_c}{\partial A_k}, \quad (2)$$

all attention mappings A_k in the last layer of the image encoder/LLM decoder, solve for z_{answer} , where A_k represents the feature map at the coordinate point of the n^{th} channel, and the resultant derivative feature map G , $c = 1, 2, 3..n$. Reshape operations transform the sequence input into a 2D shape $H \times W$. Multiply the α weight vector by the corresponding channels of the feature map A , compute a 2D activation map:

$$F_{\text{cam}} = \text{ReLU}(\sum_k \alpha_k A_k). \quad (3)$$

Grad-CAM can visualize any activation feature map, the main purpose of the paper is to explain the potential reasons behind the decisions made by the neural network. The last layer’s feature maps contain rich high-level semantic information and detailed spatial information, while the fully connected layer completely loses spatial information.

3.1.1 Grad-CAM for exploring information flow in image encoder

We utilize Grad-CAM visualization to understand the decision-making process of the CLIP Vision Transformer within the image encoder in a complex reasoning framework. Specifically, we explore the image tokens corresponding to answer tokens (e.g., (B) *mushroom*). By focusing on the last layer of the model (i.e., the features after the last layer norm) for gradient backpropagation, we can capture the fine-grained dynamics of the decision-making mechanism and visualize the image regions that the model relies on when predicting answer options (e.g., A, B, C, D).

As shown in Fig. 3, the shallow layers of the CLIP-ViT model capture general image features and broad regions of interest. The deeper layers provide key visual cues when predicting answer tokens. Attention is focused on specific regions of the images. The feature maps of these layers highlight image regions that are effective in answering the question (e.g., *mushroom*, *copoped*), indicating that the deeper layers of the CLIP-ViT are crucial for output token, and the aggregation of information flows in CLIP-Vit is mainly concentrated in the deep layer.

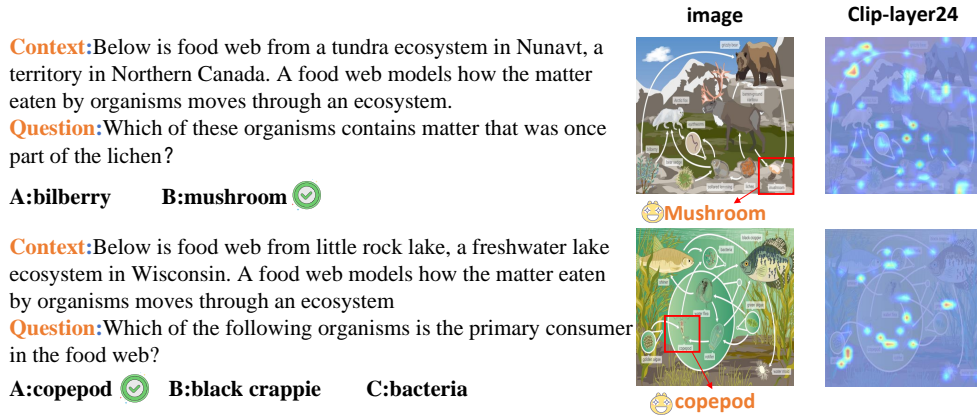


Figure 3: The Grad-CAM results of Clip-Vit (layer1-24).

Since the image encoder does not directly interact with the text, the features passing through it retain their richness. This implies that all these features contribute to generating the answer in the output stage.

3.1.2 Grad-CAM for exploring information flow in LLM decoder

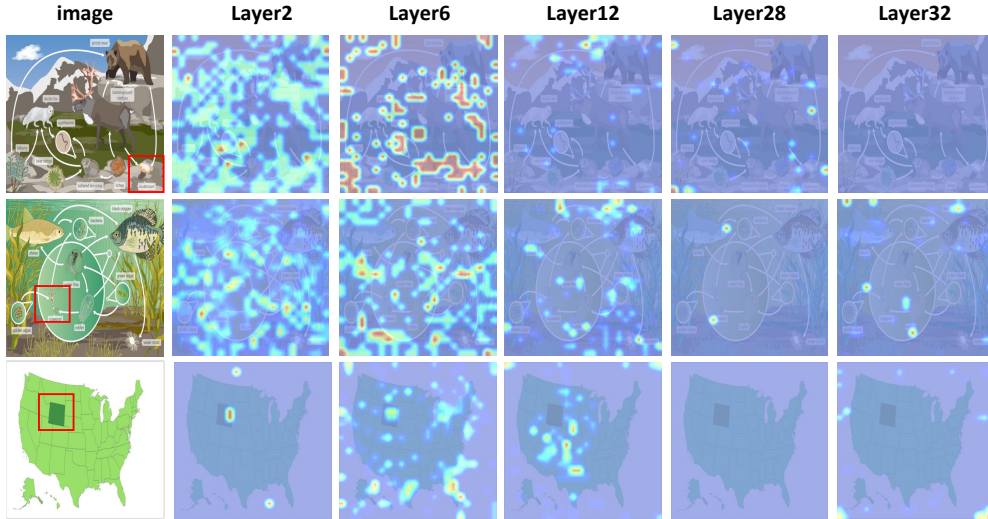


Figure 4: The Grad-CAM results of LLM(layer1-32).

The abundant features in the CLIP-ViT are passed into the LLM decoder which interacts with the text. We use Grad-CAM to visualize the information flow of image tokens and their impact on answer tokens in the LLM decoder. As shown in Fig. 4:

(1) In the shallow layers (1-11), the activation map shows significant responses to image content. The image regions related to the prompt’s options exhibit high heat map strength. We can define layers 1-11 as the image semantic interaction layer, where the model filters image tokens after understanding the context, question, and options in the prompt. The model focuses on content related to the prompt, especially the options. This phenomenon of convergence of information flow in the shallow layers is very similar to human behavior when given text and relevant images, people look at the images with questions and focus on the relevant information in the images and finally answer them.

(2) In the deep layers (12-32), the activation map shows a dispersion of information flow. Compared to the shallow layer, the aggregation of the image information flow in the region associated with the

text is almost invisible. We assume that the model relies on the information gathered in the shallow layers and combines it with the knowledge from the LLM in these deep layers, reducing the impact of the image focus.

Summarizing the previous points, we can conclude that when the model faces complex reasoning, the shallow layer (1-11) serves as the image-text semantic interaction layer, where the information flow mainly converges. The deep layer (12-32) serves as the knowledge reasoning layer, and there is no information flow converges.

3.2 Attention-score for exploring information flow in LLM decoder

In the above section, we employed Grad-CAM to visualize the contribution of the image token to the output token. To validate the observed phenomenon of shallow feature convergence highlighted in Grad-CAM, we undertake the measurement of shallow salient features through attention-score computation. This method enables us to comprehend the model’s selection and weighting mechanisms, elucidating their role in the final output. We can denote the attention score of all the tokens in the output token as the influence rate, denoted by w . This measure can be aggregated for different types of input tokens. For the output token of the complex reasoning task such as the ScienceQA dataset [35], in the n -th layer, we define \mathcal{G} as the indices set of all tokens and \mathcal{G} can be divided into three parts that represent the indices set of system, image, and user tokens:

$$\mathcal{G} = \mathcal{S} + \mathcal{I} + \mathcal{U}, \quad (4)$$

where $\mathcal{S} = \{1, \dots, N_{\text{sys}}\}$ represents the index of system token, N_{sys} represents the length of system token, $\mathcal{I} = \{N_{\text{sys}} + 1, \dots, N_{\text{sys}} + N_{\text{img}}\}$ represents the index of image token, N_{img} represents the length of image token, and $\mathcal{U} = \{N_{\text{sys}} + N_{\text{img}} + 1, \dots, N_{\text{sys}} + N_{\text{img}} + N_{\text{user}}\}$ represents the index of user token, N_{user} represents the length of user token. $A_{i,j}$ is defined as the total attention score of the output token’s attention on different types of tokens. For the i -th query token, the attentions from system, image, and user tokens are summed as 1:

$$\sum_{j \in \mathcal{S}} A_{i,j} + \sum_{j \in \mathcal{I}} A_{i,j} + \sum_{j \in \mathcal{U}} A_{i,j} = 1, \quad (5)$$

to ensure that the sum of attention scores for each token is 1, it is necessary to normalize the above summation results to calculate the total attention score for the image token:

$$\lambda_{\text{img}}^j = \sum_{j \in \mathcal{I}} A_{i,j}. \quad (6)$$

There are 576 image tokens in LLaVA1.5 and 256 image tokens in Qwen-VL. From Fig. 2(b), we can see that image tokens account for most of the input tokens, but they receive significantly less attention, instead, system prompt, which provides the least semantic information, attracts the most attention scores, and a lot of the information from image tokens is aggregated into non-image tokens such as system and user tokens, which results in the extremely inefficient visual attention in MLLMs. The sum of the image token influence on reasoning tokens in the later layers is almost zero; this objectively proves that there is information flow in the deeper layers.

3.3 Early layer truncation

As section 3.1.2 and section 3.2 mentioned, we observe the information flow of the image token showing aggregation in the shallow layers. Meanwhile, we observe that the LLM focuses on image regions relevant to the prompt and irrelevant regions in shallow interactions. The features enriched in the image encoder are fed into the LLM to engage in text interaction. At the shallow layer, the features unrelated to the text also make significant contributions, which can be detrimental to the complex reasoning task as they distract the model’s focus. This leads us to speculate whether these irrelevant features are redundant during the shallow level of interaction. Do the features fed into the LLM contain significant noise and interference, potentially leading to redundancy and interference in the features input to the LLM decoder?

To explore the phenomenon of redundancy, we design the truncation technique using the following strategy as shown in Fig. 5. In the attention matrix, each row represents the attention score of a

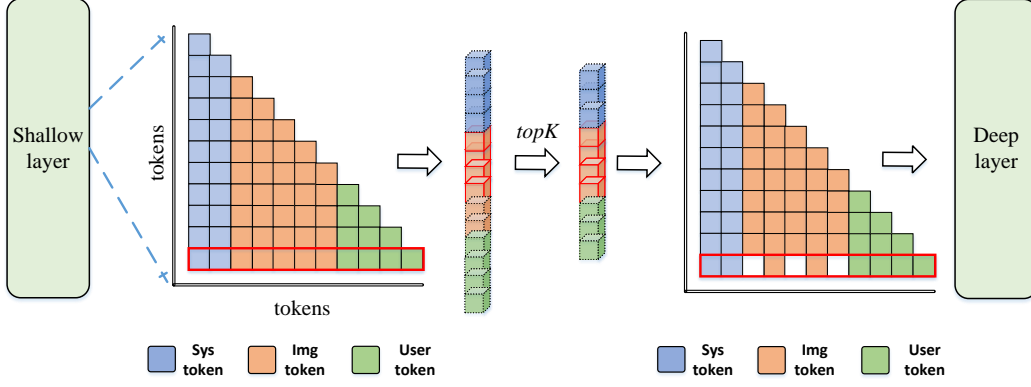


Figure 5: The diagram of attention-score truncation.

query token to all key tokens. Let H represent the number of attention heads, and S is the length of the sequence. The average attention A across different heads of the l_{th} layer attention map O is computed as:

$$A = \frac{1}{H} \sum_{h=1}^H O_h, \quad (7)$$

From this vector, we select the indices of the tokens with the highest attention scores within specific ranges. Then the corresponding attention vector segments are defined as:

$$A_{img} = A_{N_{sys}+N_{img},J} \quad (8)$$

where $A_{i,\mathcal{K}} \in \mathbb{R}^{|\mathcal{K}|}$ represents the vector composed of elements whose row index is i and column indices belong to the set \mathcal{K} , $|\mathcal{K}|$ is the element number of the set \mathcal{K} .

$$A_{i,\mathcal{K}} = [A_{i,k_1}, A_{i,k_2}, \dots] \in \mathbb{R}^{|\mathcal{K}|}, \quad \mathcal{K} = \{k_1, k_2, \dots\} \quad (9)$$

$$J' = N_{sys} + \text{argtop}(A_{img}, k), \quad (10)$$

where $\text{argtop}(\cdot, k)$ represents the function of obtaining the indices of the top k elements. The above equation 4 becomes as follows:

$$\mathcal{G}' = \mathcal{S} + J' + \mathcal{U}. \quad (11)$$

Specific truncation experiments can be found in section 4.2, the accuracy of the truncation experiments improves, demonstrating that there is redundancy in the image tokens within the LLM shallow layer interaction. This redundancy may be due to the abundance of incoming features from the image encoder, as well as the retention of features not relevant to the answer during the shallow image-text interaction in the LLM. By removing this redundancy, the model can focus solely on the relevant features.

4 Experiment

4.1 Dataset and implementation details

The ScienceQA [35] dataset is currently the only dataset available for complex CoT reasoning, containing 21,208 multimodal questions (both visual and textual), along with corresponding answers, background knowledge (lectures), and explanations. Our experiments were conducted on an A100 GPU. It is noteworthy that the current multimodal large models typically use *model.generate* for inference, allowing the inclusion of parameters such as beam search and temperature. In this paper, we utilize *model* in the replication of LLaVA1.5, defaulting to greedy search to avoid interference from other parameters.

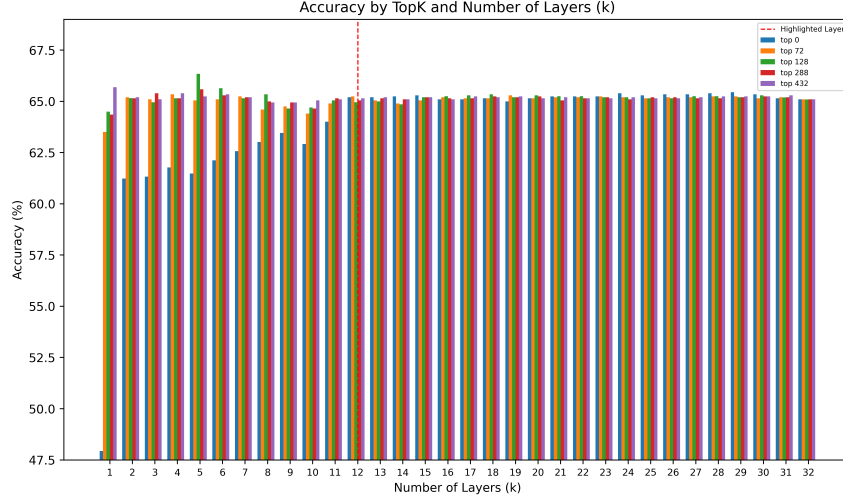


Figure 6: The truncate results of Topk on image tokens.

4.2 Redundancy truncation experiment in shallow layers

As we concluded in the previous section 3.1.2 and section 3.3, the abundant features are passed into the LLM leading to significant distraction and information flow from irrelevant features. As shown in Fig. 6, to explore the saliency and information flow of image tokens in the shallow layer, we designed an early truncation strategy. We ranked the attention scores and selected the top K image tokens to pass through, simplifying the inference process by focusing on these key tokens. We applied this attention-score truncation strategy with different values of K: 0, 72, 128, 244, and 432.

(1) When the layer=1, k=0, there is no image token passed to the LLM, while the LLM can surprisingly achieve an accuracy of 47.5 %, which suggests that in some scenarios the LLM relies only on the text to answer the questions on their own through prior knowledge, such as ‘What is the capital of Nebraska?’ in Fig. 7. Therefore, LLM does not attend to graphical information when LLM’s knowledge can directly answer a question.

(2) When the layer=1, k=432, the accuracy was found to be improved by 0.6 points (baseline: 65.00%). This suggests that image features passed by Clip-ViT are redundant for LLM, because clip-vit has limited perceptual ability for fine-grained recognition requirements, and cannot maintain beneficial features after image encoder compression, resulting in redundancy and interference.

(3) When the layer=5, k=128, the accuracy rate achieved the highest by 66.48%.

(4) When the layer>=12, the accuracy still retains 65.00% even with 0 image tokens. This suggests that image tokens play little role in the performance of the model. This figure supports our hypothesis again that there is no information flow between the deep layers.

In summary, the truncation experiments once again validate the two conclusions of this paper that when facing complex reasoning tasks (1) image and text interaction occurs in the shallow (1-11) layer, while no information flow of image and text interacts in the deep layer. (2) In the shallow layer, there is a part of redundancy in the image features, and the truncation experiment proposed in this paper helps to remove some of the redundant features.

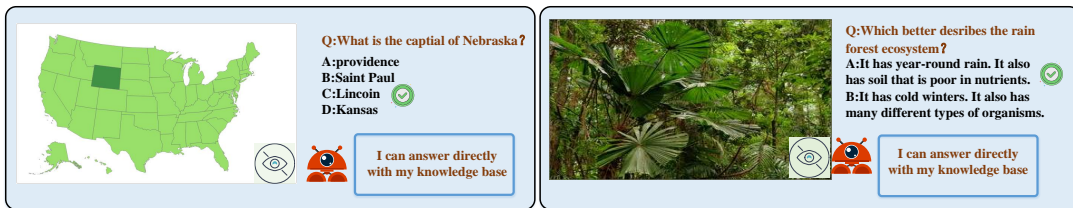


Figure 7: It shows the case lacks visual dependency.

Table 1: Comparison among different MLLMs on ScienceQA benchmarks, “Res” represents the input image resolution.

Method	Model	LLM backbone	Res	SQA(IMG)%
Instruct-BLIP [6]	Zero-shot	Vicuna-7B	224	60.50
Instruct-BLIP [6]	Zero-shot	Vicuna-13B	224	63.10
BLIP-2 [11]	Zero-shot	Vicuna-13B	224	61.03
Shikra [27]	Zero-shot	Vicuna-13B	224	45.80
DDCoT(GPT3.5) [37]	Zero-shot	175B	-	72.53
DDCoT(MiniGPT-4) [37]	Zero-shot	Vicuna-13B	-	56.72
Ying-VLM [38]	Zero-shot	-	-	55.70
Otter [40]	Zero-shot	-	-	66.30
MiniGPT-4 [14]	Zero-shot	Vicuna-13B	336	42.34
Qwen-VL-Chat [13]	Zero-shot	Qwen-7B	448	68.21
MobileVLM [16]	Zero-shot	MobileLLaMA	336	61.00
Qwen-VL [13]	Zero-shot	Qwen-7B	448	67.12
LLaVA1.5 [2]	Zero-shot	Vicuna-7B	336	65.00
LLaVA1.5 + Ours	Zero-shot	Vicuna-7B	336	66.48
LLaVA1.5[2]	Zero-shot	Vicuna-13B	336	71.60
LLaVA1.5 + Ours	Zero-shot	Vicuna-13B	336	72.85

4.3 Ablation study of truncation strategy

To verify the generalization of the phenomenon of information flow convergence during complex reasoning tasks, we have done experiments on both Qwen and LLaVA1.5. It is very interesting that the aggregation in shallow layers also occurs in Qwen and LLaVA1.5. The visual results are shown in Table 1, we applied the truncation technique to Qwen-VL and LLaVA1.5, and compared it with other CoT methods. Our method proved effective in both Qwen-VL and LLaVA1.5, further highlighting the importance of image tokens in shallow layers. This also suggests that MLLMs might be more adept at capturing specific patterns or structures in the input data during the shallow layers, while relying on the LLM’s inherent knowledge for reasoning at deep layers.

4.4 Qualitative study of prompt

Table 2: Compare results of Prompt position of CoT (baseline:LLaVA-1.5-7B).

Prompt position	Method	LLM-decoder	SQA(IMG)%
QCM-A	Zero-shot	greedy search	46.06
P1-CQM-A	Zero-shot	greedy search	59.49
CQM-P1-A	Zero-shot	greedy search	57.36
CQM-P2-A	Zero-shot	greedy search	64.65
CQM-P3-A	Zero-shot	greedy search	63.36
CQM-A	Zero-shot	beam search(n=5)	58.54
	Zero-shot	beam search(n=4)	59.64
	Zero-shot	beam search(n=3)	60.98
	Zero-shot	beam search(n=2)	63.16
	Zero-shot	greedy search(n=1)	65.00

First, we investigated the position of prompts, using various configurations such as QCM-A, P-QCM-A, QCM-P-A, and CQM-A, where Q stands for question, C for context, M for options, and A for answer. We carried out experiments with four kinds of prompts within the Chain-of-Thought (CoT) framework. As shown in Table 3, P1 adopts the two-stage prompt of DDCoT [37], such as: *"Given the context, questions, and options, please think step-by-step to answer the question, deconstruct the problem as completely as possible down to necessary sub-questions. Then, to help humans answer the original question, try to answer the sub-questions"*.

P2 is: *"Given the context, questions, and options, please think step-by-step to answer the question"*.
P3 is: *"Please think step-by-step and answer with the option’s letter from the given choices directly"*.

In our experiments, we discovered that incorporating zero-shot CoT prompts, typically used in LLMs, adversely affected the LLaVA-1.5 model, rendering the original CQM-A prompt the most effective. Furthermore, when comparing beam search and greedy search, we found that the CQM-A setup with greedy search yielded the optimal performance.

4.5 Grad-CAM results of different prompt

In this section, we explored the variation of heat maps under different prompts. As shown in Fig.10, our experiments indicate that when the prompt involves a simple VQA (Visual Question Answering) task, the heat map consistently focuses on the relevant areas from layer 1 through layer 32. Meanwhile, when the prompt requires complex reasoning that integrates textual information, we observe the convergence of shallow information flow, as discussed in this paper. Notably, deep information flow remains less pronounced under these conditions.

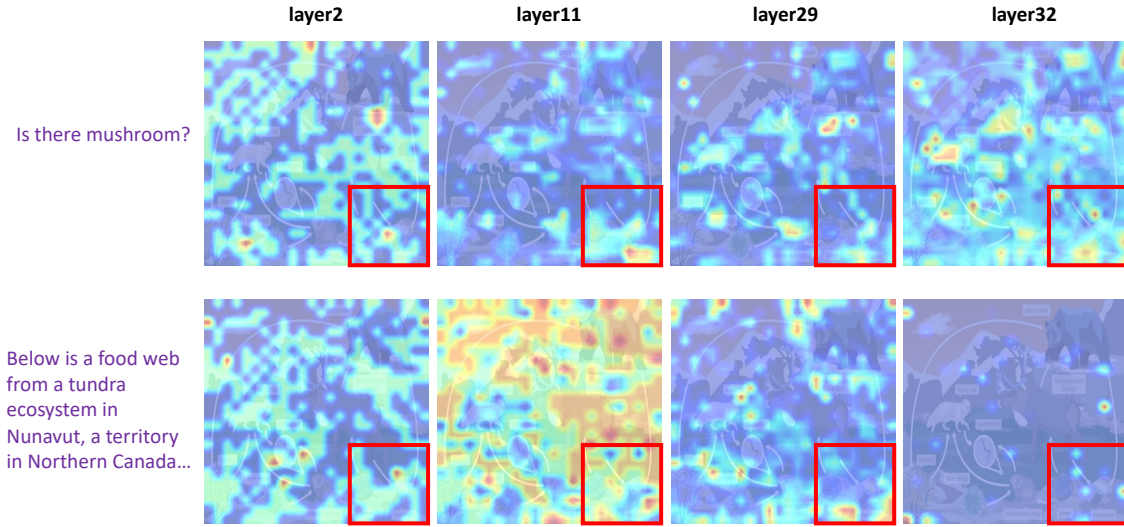


Figure 8: The Grad-CAM results of different prompts (complex reasoning and visual question answer).

5 Grad-CAM results of truncation strategy

This section also compared the heat maps before and after truncation. As shown in Fig.11, the information flow converges on relevant and irrelevant features before truncation. Consequently, after applying attention-score truncation, the convergence on irrelevant features significantly decreases. This reduction allows the model to focus more effectively on the relevant areas of the image. This improvement in focus highlights the benefits of eliminating redundant features, thereby enhancing the model's performance and accuracy.

6 limitations

Grad-CAM is primarily used to provide a visual interpretation by visualizing the gradient information at a particular layer that shows the image regions the model focuses on when making predictions. While this is useful for understanding the interaction mechanisms between image and text, it may not be sufficient to fully capture textual components' complex interaction and reasoning processes. Attention scores can reveal what the model focuses on when processing input, but they are static and do not fully reflect the dynamics of the model throughout the reasoning process. Our demonstration of redundancy in image features and aggregation of image tokens over salient tokens through truncation techniques also reveals an important issue: even with advanced visualization and interpretation

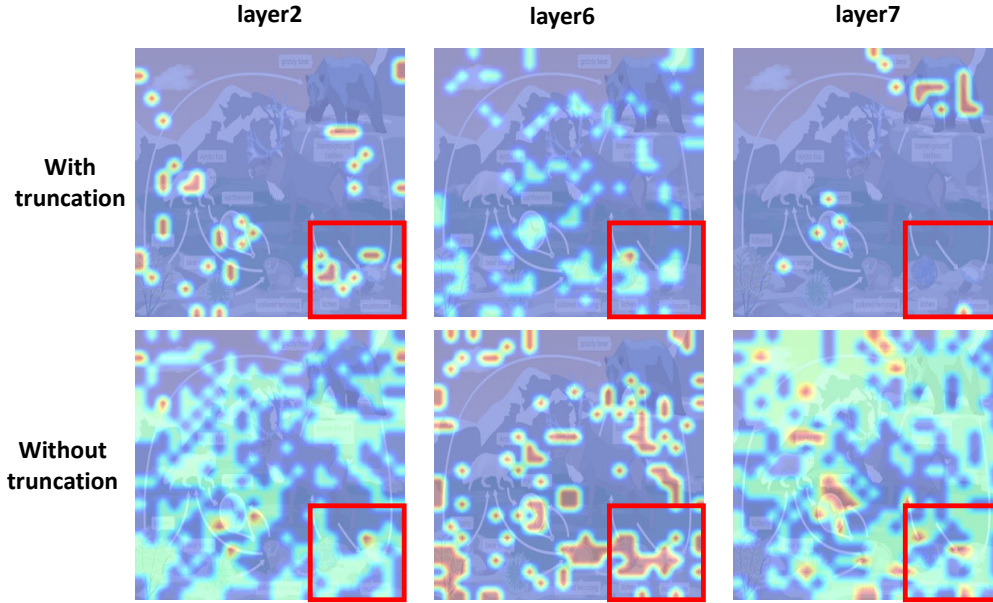


Figure 9: The Grad-CAM results of truncation strategy.

methods, it remains a challenge to effectively handle and reduce information redundancy to improve model efficiency and interpretability.

7 Conclusion

In this paper, we employ Grad-CAM to visualize the complex reasoning processes layer-by-layer within Multimodal Large Language Models (MLLMs) and to investigate the dynamics of interaction and information flow between images and user prompts. Our findings indicate a significant confluence of information flow in the shallow layers, particularly in models such as LLaVA1.5 and Qwen-vl, where we observed a notable redundancy in the image tokens’ information flow at these shallow layers. To address this issue, we introduced a truncation strategy aimed at concentrating image tokens around the most relevant or ‘salient’ tokens. Our experimental results confirm that this approach achieves a consistent improvement in performance. We hope that this work will help people understand the mechanism of multimodal complex reasoning.

References

- [1] Liu H, Li C, Wu Q, et al. Visual instruction tuning[J]. Advances in neural information processing systems, 2024, 36.
- [2] Liu H, Li C, Li Y, et al. Improved baselines with visual instruction tuning[J]. arXiv preprint arXiv:2310.03744, 2023.
- [3] Liu H, Li C, Li Y, et al. Llava-next: Improved reasoning, ocr, and world knowledge[J]. 2024.
- [4] Zhang Z, Zhang A, Li M, et al. Multimodal chain-of-thought reasoning in language models[J]. arXiv preprint arXiv:2302.00923, 2023.
- [5] Alayrac J B, Donahue J, Luc P, et al. Flamingo: a visual language model for few-shot learning[J]. Advances in neural information processing systems, 2022, 35: 23716-23736.
- [6] Dai W, Li J, Li D, et al. Instructblip: Towards general-purpose vision-language models with instruction tuning[J]. Advances in Neural Information Processing Systems, 2024, 36.
- [7] Wang L, Li L, Dai D, et al. Label words are anchors: An information flow perspective for understanding in-context learning[J]. arXiv preprint arXiv:2305.14160, 2023.

- [8] Zhang Y, Qian S, Peng B, et al. Prompt Highlighter: Interactive Control for Multi-Modal LLMs[J]. arXiv preprint arXiv:2312.04302, 2023.
- [9] Todd E, Li M L, Sharma A S, et al. Function vectors in large language models[J]. arXiv preprint arXiv:2310.15213, 2023.
- [10] Selvaraju R R, Cogswell M, Das A, et al. Grad-cam: Visual explanations from deep networks via gradient-based localization[C]//Proceedings of the IEEE international conference on computer vision. 2017: 618-626.
- [11] Li, Junnan, et al. "Blip-2: Bootstrap** language-image pre-training with frozen image encoders and large language models." International conference on machine learning. PMLR, 2023.
- [12] Dai D, Dong L, Hao Y, et al. Knowledge neurons in pretrained transformers[J]. arXiv preprint arXiv:2104.08696, 2021.
- [13] Bai J, Bai S, Yang S, et al. Qwen-vl: A versatile vision-language model for understanding, localization, text reading, and beyond[J]. 2023.
- [14] Zhu D, Chen J, Shen X, et al. Minigpt-4: Enhancing vision-language understanding with advanced large language models[J]. arXiv preprint arXiv:2304.10592, 2023.
- [15] Zhang P, Wang X D B, Cao Y, et al. Internlm-xcomposer: A vision-language large model for advanced text-image comprehension and composition[J]. arXiv preprint arXiv:2309.15112, 2023.
- [16] Chu, **angxiang, et al. "Mobilevlm: A fast, reproducible and strong vision language assistant for mobile devices." arxiv preprint arXiv:2312.16886 (2023).
- [17] Wang W, Lv Q, Yu W, et al. Cogvlm: Visual expert for pretrained language models[J]. arXiv preprint arXiv:2311.03079, 2023.
- [18] Li Z, Yang B, Liu Q, et al. Monkey: Image resolution and text label are important things for large multi-modal models[J]. arXiv preprint arXiv:2311.06607, 2023.
- [19] Li Y, Wang C, Jia J. LLaMA-VID: An image is worth 2 tokens in large language models[J]. arXiv preprint arXiv:2311.17043, 2023.
- [20] Lin B, Tang Z, Ye Y, et al. Moe-llava: Mixture of experts for large vision-language models[J]. arXiv preprint arXiv:2401.15947, 2024.
- [21] Young A, Chen B, Li C, et al. Yi: Open foundation models by 01. ai[J]. arXiv preprint arXiv:2403.04652, 2024.
- [22] Li Y, Zhang Y, Wang C, et al. Mini-Gemini: Mining the Potential of Multi-modality Vision Language Models[J]. arXiv preprint arXiv:2403.18814, 2024.
- [23] Yang R, Song L, Li Y, et al. Gpt4tools: Teaching large language model to use tools via self-instruction[J]. Advances in Neural Information Processing Systems, 2024, 36.
- [24] Zhang H, Li X, Bing L. Video-llama: An instruction-tuned audio-visual language model for video understanding[J]. arXiv preprint arXiv:2306.02858, 2023.
- [25] Maaz M, Rasheed H, Khan S, et al. Video-chatgpt: Towards detailed video understanding via large vision and language models[J]. arXiv preprint arXiv:2306.05424, 2023.
- [26] Lyu C, Wu M, Wang L, et al. Macaw-llm: Multi-modal language modeling with image, audio, video, and text integration[J]. arXiv preprint arXiv:2306.09093, 2023.
- [27] Chen K, Zhang Z, Zeng W, et al. Shikra: Unleashing Multimodal LLM's Referential Dialogue Magic[J]. arXiv preprint arXiv:2306.15195, 2023.
- [28] Lai X, Tian Z, Chen Y, et al. Lisa: Reasoning segmentation via large language model[J]. arXiv preprint arXiv:2308.00692, 2023.
- [29] Han J, Zhang R, Shao W, et al. Imagebind-llm: Multi-modality instruction tuning[J]. arXiv preprint arXiv:2309.03905, 2023.

- [30] Chen J, Zhu D, Shen X, et al. Minigpt-v2: large language model as a unified interface for vision-language multi-task learning[J]. arXiv preprint arXiv:2310.09478, 2023.
- [31] Chu Z, Chen J, Chen Q, et al. A survey of chain of thought reasoning: Advances, frontiers and future[J]. arXiv preprint arXiv:2309.15402, 2023.
- [32] Zellers R, Bisk Y, Farhadi A, et al. From recognition to cognition: Visual commonsense reasoning[C]//Proceedings of the IEEE/CVF conference on computer vision and pattern recognition. 2019: 6720-6731.
- [33] Park J S, Bhagavatula C, Mottaghi R, et al. Visualcomet: Reasoning about the dynamic context of a still image[C]//Computer Vision–ECCV 2020: 16th European Conference, Glasgow, UK, August 23–28, 2020, Proceedings, Part V 16. Springer International Publishing, 2020: 508-524.
- [34] Dong Q, Qin Z, Xia H, et al. Premise-based multimodal reasoning: Conditional inference on joint textual and visual clues[J]. arXiv preprint arXiv:2105.07122, 2021.
- [35] Lu P, Mishra S, Xia T, et al. Learn to explain: Multimodal reasoning via thought chains for science question answering[J]. Advances in Neural Information Processing Systems, 2022, 35: 2507-2521.
- [36] Zhang Z, Zhang A, Li M, et al. Multimodal chain-of-thought reasoning in language models[J]. arXiv preprint arXiv:2302.00923, 2023.
- [37] Zheng G, Yang B, Tang J, et al. Ddcot: Duty-distinct chain-of-thought prompting for multimodal reasoning in language models[J]. Advances in Neural Information Processing Systems, 2023, 36: 5168-5191.
- [38] Li, Lei, et al. "M³ IT: A Large-Scale Dataset towards Multi-Modal Multilingual Instruction Tuning." arxiv preprint arXiv:2306.04387 (2023).
- [39] Shao H, Qian S, Xiao H, et al. Visual CoT: Unleashing Chain-of-Thought Reasoning in Multi-Modal Language Models[J]. arXiv preprint arXiv:2403.16999, 2024.
- [40] Zhao, Haozhe, et al. "Mmicl: Empowering vision-language model with multi-modal in-context learning." arxiv preprint arXiv:2309.07915 (2023).
- [41] Huang Q, Dong X, Zhang P, et al. Opera: Alleviating hallucination in multi-modal large language models via over-trust penalty and retrospection-allocation[J]. arXiv preprint arXiv:2311.17911, 2023.
- [42] Chen L, Zhao H, Liu T, et al. An Image is Worth 1/2 Tokens After Layer 2: Plug-and-Play Inference Acceleration for Large Vision-Language Models[J]. arXiv preprint arXiv:2403.06764, 2024.

A Qualitative study of prompt

Table 3: Compare results of Prompt position of CoT (baseline:LLaVA-1.5-7B).

Prompt position	Method	LLM-decoder	SQA(IMG)%
QCM-A	Zero-shot	greedy search	46.06
P1-CQM-A	Zero-shot	greedy search	59.49
CQM-P1-A	Zero-shot	greedy search	57.36
CQM-P2-A	Zero-shot	greedy search	64.65
CQM-P3-A	Zero-shot	greedy search	63.36
CQM-A	Zero-shot	beam search(n=5)	58.54
	Zero-shot	beam search(n=4)	59.64
	Zero-shot	beam search(n=3)	60.98
	Zero-shot	beam search(n=2)	63.16
	Zero-shot	greedy search(n=1)	65.00

First, we investigated the position of prompts, using various configurations such as QCM-A, P-QCM-A, QCM-P-A, and CQM-A, where Q stands for question, C for context, M for options, and A for answer. We carried out experiments with four kinds of prompts within the Chain-of-Thought (CoT) framework. As shown in Table 3, P1 adopts the two-stage prompt of DDCoT [37], such as: *"Given the context, questions, and options, please think step-by-step to answer the question, deconstruct the problem as completely as possible down to necessary sub-questions. Then, to help humans answer the original question, try to answer the sub-questions"*.

P2 is: *"Given the context, questions, and options, please think step-by-step to answer the question"*. P3 is: *"Please think step-by-step and answer with the option's letter from the given choices directly"*. In our experiments, we discovered that incorporating zero-shot CoT prompts, typically used in LLMs, adversely affected the LLaVA-1.5 model, rendering the original CQM-A prompt the most effective. Furthermore, when comparing beam search and greedy search, we found that the CQM-A setup with greedy search yielded the optimal performance.

B Grad-CAM results of different prompt

In this section, we explored the variation of heat maps under different prompts. As shown in Fig.10, our experiments indicate that when the prompt involves a simple VQA (Visual Question Answering) task, the heat map consistently focuses on the relevant areas from layer 1 through layer 32. Meanwhile, when the prompt requires complex reasoning that involves integrating textual information, we observe the convergence of shallow information flow, as discussed in this paper. Notably, the phenomenon of deep information flow remains less pronounced under these conditions.

C Grad-CAM results of truncation strategy

In this section, we also compared the heat maps before and after truncation. As shown in Fig.11, before truncation, the information flow converges on both relevant and irrelevant features. Consequently, after applying attention-score truncation, the convergence on irrelevant features significantly decreases. This reduction allows the model to focus more effectively on the relevant areas of the image. This improvement in focus highlights the benefits of eliminating redundant features, thereby enhancing the model's performance and accuracy.

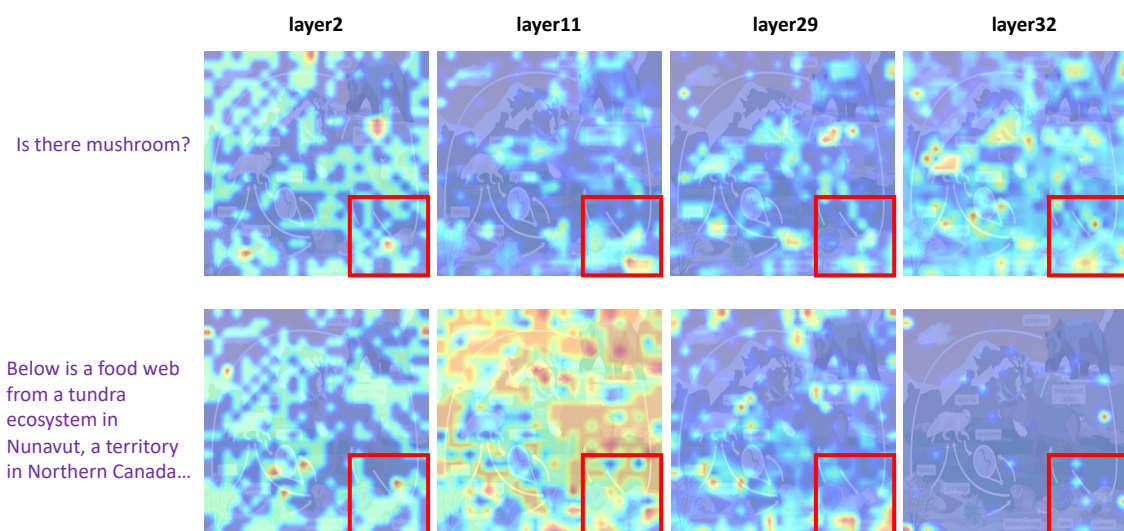


Figure 10: The Grad-CAM results of different prompts (complex reasoning and visual question answer).

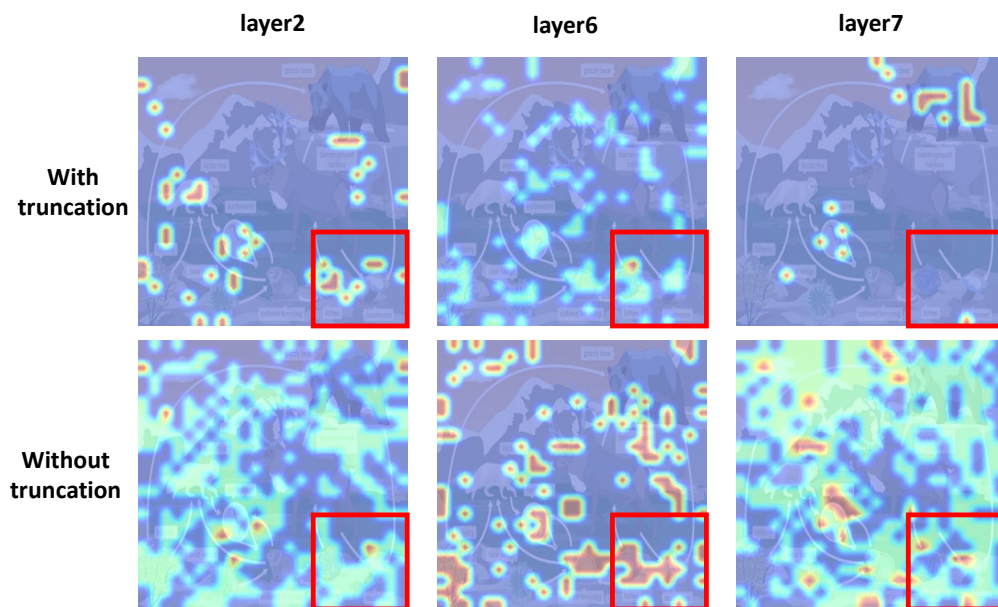


Figure 11: The Grad-CAM results of truncation strategy.